

A Solid-State Hyperspectral Imager for Real-time Standoff Explosives Detection using Shortwave Infrared Imaging

Bora M. Onat^{*}, Gary Carver, Mark Itzler
Princeton Lightwave Inc., 2555 US 130, Suite A, Cranbury NJ, USA 08512

ABSTRACT

We present a new and innovative short-wave infrared (SWIR) hyperspectral imaging focal plane array (FPA) concept for bulk and trace standoff explosives detection. The proposed technology combines conventional uncooled InGaAs based SWIR imaging with the wavelength selectivity of a monolithically integrated solid-state Fabry-Perot interferometer. Each pixel of the array consists of a group of sub-pixels in which each sub-pixel is tuned to absorb a separate wavelength. The relative responses from the sub-pixels (i.e. wavelengths) are compared to the spectral characteristics of explosives in the SWIR to detect and locate them within an imaged scene among various background materials.

The novel technology will be compact, and consume low power such that it can be used as a handheld device or mounted for persistent surveillance of crowded areas and checkpoints. The technology does not use any scanning nor tuning apparatuses such as MEMS devices, and is therefore fast, compact, lightweight and not susceptible to vibration. The technology is therefore ideal for man portable applications and unmanned vehicle platforms. An eyesafe (covert) illuminator may be used to provide illumination in situations when ambient light conditions are not sufficient. We will present a detailed design of the novel focal plane array and a theoretical standoff distance and false rates study.

Keywords: InGaAs, Shortwave infrared, imaging, focal plane array, standoff explosives detection, hyperspectral.

1. INTRODUCTION

There is a vital and urgent need for standoff explosive detection (SED) systems that can be used in airport check points, crowd monitoring at public events, border security, and baggage screening. Such an approach must have large standoff distances so imminent threats can be detected and prevented before causing damages and casualties to the public. Terahertz-wave imaging techniques have shown promising results in displaying hidden threats under clothing, but require high power sources and display details of body areas that raise privacy concerns when used on the general public [1]. Thermal imaging techniques have been used to detect concealed weapons under clothing, however exhibit difficulty when many layers are worn during cold temperatures [2]. Although these techniques are most effective in detecting concealed metal objects, another complementary technology is needed to assess and correctly identify a possible imminent threat.

Trace amounts of explosive material particles (EP) adhere to the skin, clothing and possessions of individuals who have handled them [1]. Since the most thorough clean up has difficulty in removing these microscopic trace amounts, new technologies have emerged to exploit this property. Hyperspectral Electro-Optical (E-O) based technologies have shown promise in bulk and trace explosives detection from a standoff distance. These methods rely on seeking the specific optical properties of EPs in an imaged scene among other background materials. It is highly desirable that the sensor/system have high sensitivity, low false alarm rates, and real time operation.

Spectroscopy based hyperspectral detection techniques have demonstrated detecting EPs from 15-20 ft using ambient light conditions [3]. Recent advances in laser-based explosives detection have proposed Raman

^{*} bmonat@princetonlightwave.com; phone 1 609 495 2546; fax 1 609 395 9113; www.princetonlightwave.com

Spectroscopy, Laser induced fluorescence spectroscopy or photoluminescence spectroscopy [3]. These technologies require pulsed laser power to be directed at the object in the visible-near IR wavelength ranges (248nm, 532nm, & 785nm). Fourier Transform spectrometer based hyperspectral techniques have demonstrated capability of detecting chemical agents in an imaged scene [5] and could potentially be used for stand-off explosives detection as well. However, all of the above technologies require discrete bulky components such as diffraction gratings, mirrors and precision mounted optics that increase the complexity, size, weight and cost of the system. In addition, laser-based techniques can not be used to screen the general public at security check points due to eye safety concerns.

We propose a novel bulk and trace SED system that utilizes a truly unique electro-optical (E-O) sensor which is based on the mature InGaAs focal plane array (FPA) technology used to detect short-wave infrared (SWIR) radiation. The concept is based on measuring the reflected SWIR radiation of an imaged scene and comparing it to the reflected response of explosive materials. Our simulations predict high detection probabilities (~90%) with low false alarm rate (<10%) can be observed in each integration time since these materials have very distinct reflective characteristics compared to background materials such as cotton, wood, jeans, cardboard, and nylon. Our sensor has the potential for detecting explosives from a safe standoff distance in real time and has the following capabilities that make it ideal for use on unmanned vehicle platforms, a handheld device or mounted for persistent surveillance of crowded areas and checkpoints:

- Compact, robust and low power system based on uncooled FPA technology.
- Passive operation under sufficient ambient light. Otherwise, eye-safe illumination sources may be utilized which is safe for users and individuals being interrogated.
- The system is factory calibrated and does not require periodic internal or external calibrations, have extensive setup procedures, nor does it require extensive operator training.
- Not only detect the presence of EP, locate it spatially in a scene of view.
- Simulations predict high detection probabilities (~90%) with low false alarm rate (<10%) and high detection capability of explosives type (~70%).
- The sensor is all solid-state, contains no moving parts, is not MEMs based, and is therefore quiet, and not sensitive to vibration.

In this paper we will present the concept of the new technology and its design considerations. In Section 3 we will discuss the method used to simulate the detection probability and false alarm rate. In Section 4 we discuss the trade-offs between standoff capability vs. lens and FPA design.

2. PROPOSED CONCEPT TECHNOLOGY

2.1 Shortwave Infrared (SWIR) Spectroscopy

This section discusses the shortwave infrared optical physics that support our technology. Our approach is based on measuring the reflectivity of explosive materials in the SWIR at wavelengths from 1500 to 1800 nm. Black body emission peaks near 10 microns for temperatures expected in the targeted applications. As a result, in the SWIR, reflected infrared radiation will dominate thermal emission, and contrast will be caused by variations in the optical properties of the target. Contrast between objects in the infrared is often quite different than in the visible [6]. This is due to spectral variations in the real (n) and imaginary (k) parts of the refractive index. In particular, absorption bands cause large changes in both 'n' and 'k' values [7]. Many white or grey powders (as observed in the visible) exhibit pronounced absorption bands in the infrared where photon energy matches the resonance energies of molecular vibrations. Energetic materials such as RDX, HMX, and N5 exhibit several strong absorption bands in the infrared region between 2 and 10 microns [8]. As shown in Figure 1, reflection from EP display overtones in the SWIR that are much more distinctive than common background materials shown in Figure 2 [3]. These overtones are weaker than the fundamental absorption bands at longer

wavelengths, but key optical components (sources, lenses, detectors) are superior in the SWIR and leverage a mature supply base funded by years of R&D investments in the telecommunications arena.

We exploit the spectral characteristic from 1500 to 1800 nm shown in Figure 1 as it is sufficient to identify and distinguish the five shown explosive materials compared to background materials using our approach. We have elected to concentrate on the 1500 to 1800 nm wavelength range in this study since these SWIR wavelengths have low atmospheric attenuation - allowing for the opportunity of SED at distances greater than 20-50 meters. For example the water absorption band at 1460 nm (between astronomer's J and H windows) reduces transmission to about 80% through 20 meters of air at 50% relative humidity[9],[10].

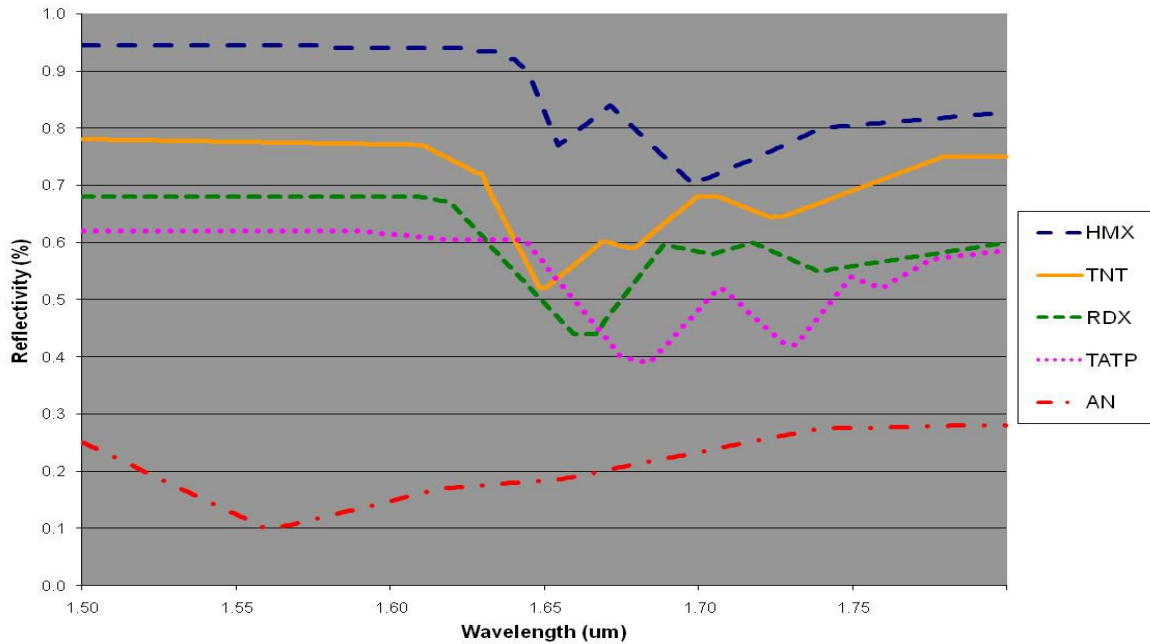


Figure 1 – SWIR reflectance of five explosive materials, after Ref [3].

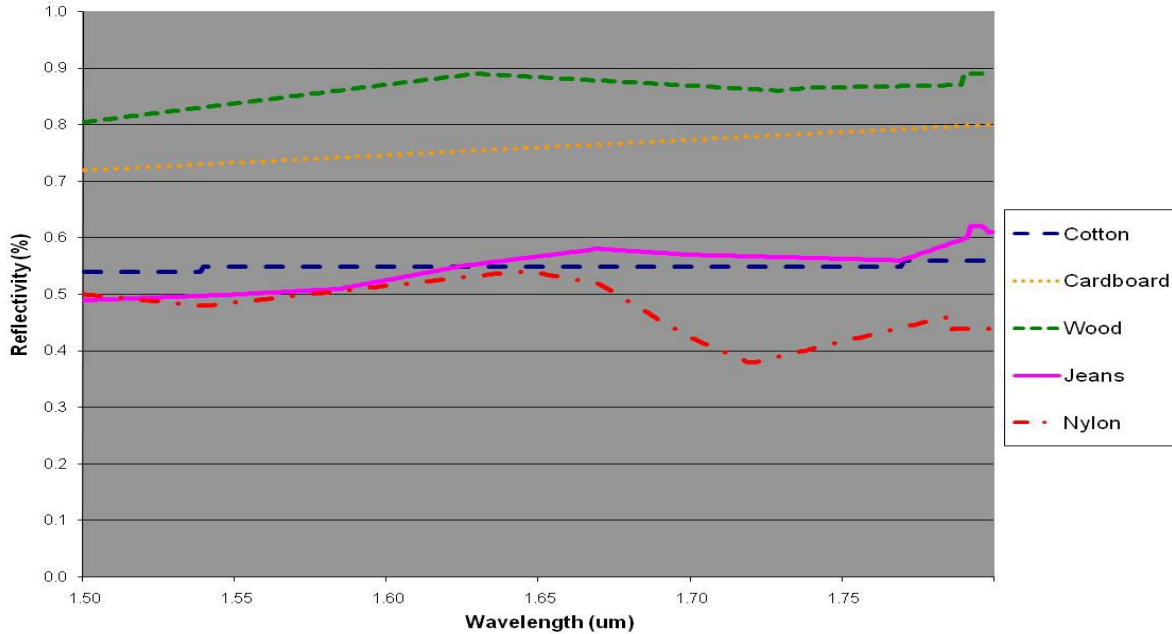
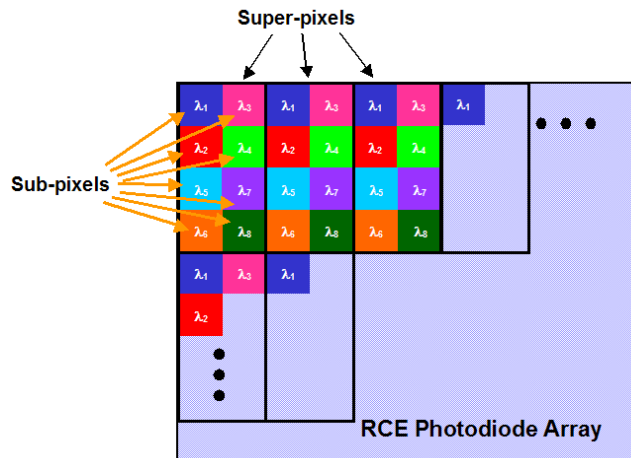


Figure 2 – SWIR reflectance of common background material, after Ref [3].

2.2 Focal Plane Array Concept

Based on the above optical physics, we present a new and innovative FPA technology that combines conventional uncooled InGaAs based SWIR imaging with the wavelength selectivity of a monolithically integrated solid-state Fabry-Perot interferometer. Each pixel of the array consists of a group of sub-pixels in which each sub-pixel is tuned to absorb a separate wavelength. The concept is illustrated in Figure 3a, showing the layout of each spectrally tuned sub-pixel in a photodiode array. The monolithic InGaAs photodiode array is hybridized to a commercial readout integrated circuit (ROIC), and each sub-pixel response is read out. The relative responses from the sub-pixels (i.e. wavelengths as shown in Figure 3b) are compared to the spectral characteristics of explosives in the SWIR to detect and locate them within an imaged scene. Figure 4 illustrates the cross-section of the FPA after the photodiode array has been indium bump hybridized to a ROIC. The sub-pixel Fabry-Perot interferometer design will be described in the next section.



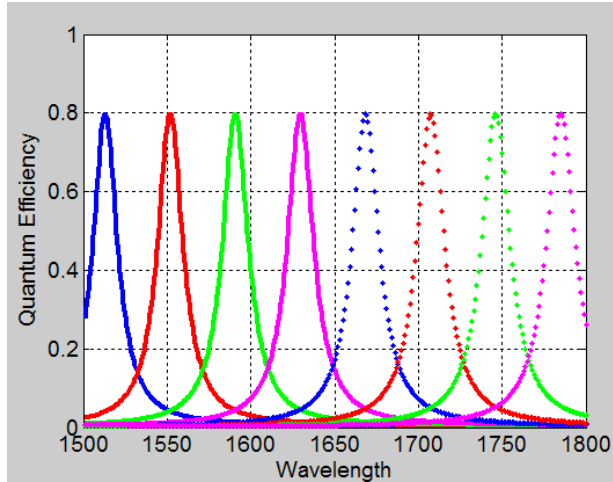


Figure 3. a) Layout of pixels in a super-pixel in a resonant cavity enhanced (RCE) photodiode array. b) Calculated spectral response of 8 pixels in an array tuned to different wavelengths in the SWIR.

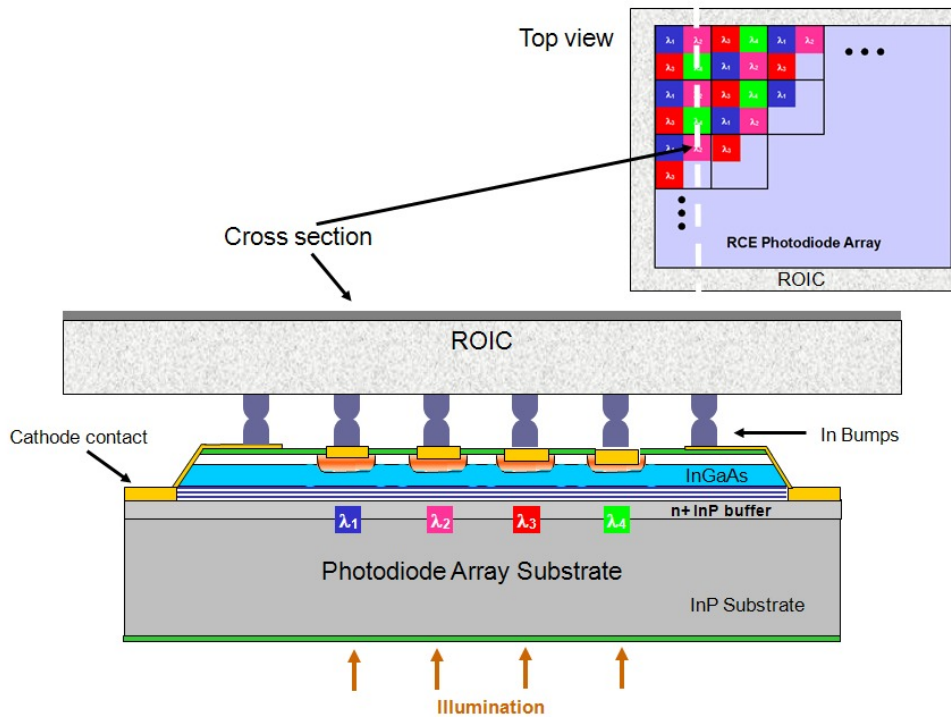


Figure 4. Cross-section of the FPA showing the photodiode array hybridized to a ROIC.

2.3 Device (sub-pixel) technology

The integration of Fabry-Perot interferometers with solid state devices was explored in the 1990s and referred to as resonant cavity enhanced (RCE) devices [11]. The RCE devices benefit from the wavelength sensitivity and the large increase of the resonant optical field introduced by the optical cavity. RCE photodiodes are constructed by integrating a thin absorber region into an asymmetric Fabry-Perot cavity. The cavity is formed by top and bottom reflectors which can be fabricated by various methods such as DBR's, metal or by using the semiconductor-air interface [12]. Since most RCE photodiodes reported to date are top-illuminated, the top reflector is typically formed by surface deposited dielectric reflectors such as silicon-dioxide/silicon-nitride distributed feedback reflectors (DBR) while the bottom reflector is an epitaxially grown semiconductor DBR. RCE photodiodes were primarily explored for telecommunication applications to enhance the responsivity and

bandwidth of photodiodes, at the expense of narrow spectral operation. After the maturity of arrayed waveguide grating devices, that can separate a wide band of wavelengths very efficiently, the RCE concept for photodiodes was abandoned.

The quantum efficiency for a RCE photodiode can be expressed as [11]

$$\eta = \frac{(1 + R_2 \times e^{-\alpha d})}{(1 - 2\sqrt{R_1 R_2} e^{-\alpha d} \cos(2\beta L + \psi_1 + \psi_2) + R_1 R_2 e^{-2\alpha d})} \times (1 - R_1)(1 - e^{-\alpha d}) \quad (1)$$

where α and d are the absorption coefficient and thickness for the thin absorber, β is the optical propagation constant, L is the length of the cavity, and R_1, ψ_1 and R_2, ψ_2 are the amplitude and phase of the first and second reflectors respectively.

At resonance, when the round trip phase shift is a multiple of 2π , the peak quantum efficiency can be calculated from equation (1):

$$\eta_p = \left(\frac{(1 + R_2 e^{-\alpha d})}{(1 - \sqrt{R_1 R_2} e^{-\alpha d})^2} \right) \times (1 - R_1)(1 - e^{-\alpha d}) \quad (2)$$

The high speed RCE photodiodes for telecommunication applications were typically top illuminated due to the ease of application of the top dielectric DBR. For 2-D imaging applications, a back illuminated RCE design is desirable, in order for the top photodiode contacts to be indium bump hybridized to a ROIC.

Our invention leverages many of the fabrication techniques of conventional InGaAs photodiode arrays and integrates it with a back illuminated RCE detection concept. The RCE photodiode sub-pixel comprises of an InP substrate and the following epitaxially grown layers: an InP buffer layer, a semiconductor DBR, an InGaAs absorber, and a high bandgap InP cap layer (Figure 5b). A conventional InGaAs photodiode is shown in Figure 5a for comparison. Since illumination is incident on the device from the substrate, the epitaxial DBR is the first reflector, and the metal contact serves as the second reflector of the cavity. The fabrication process is similar to the conventional InGaAs photodiode with the exception that the InP cap layer will be etched (varying from sub-pixel to sub-pixel) using standard photolithography techniques to vary the optical cavity length L in equation (1), effectively tuning the cavity. Consequently, sub-pixels will be selectively tuned to detect a narrow wavelength band within a wavelength spectrum of interest during fabrication (see Figure 3b). The free spectral range of the cavity is designed such that 2nd and higher order cavity resonances occur either above the InGaAs absorption band (> 1800 nm) or below 1500 nm. A high pass 1500 nm filter will be used in the optical system. As additional design flexibility, a dielectric DBR may be used instead of a epitaxial grown semiconductor DBR for wider spectral window with high reflectivity. This requires the InP substrate being removed post hybridization, and the semiconductor DBR deposited on the backside both of which are common semiconductor processing techniques.

Also apparent in Figure 5, is that the RCE photodiode's InGaAs absorber region is thinner compared to conventional photodiode. This is due to the fact that resonant enhancement of the device allows the use of thin absorber layers and can yet achieve very high quantum efficiency [11]. Based on our initial calculations, an InGaAs thickness of only ~ 0.2 μm (compared to $3\mu\text{m}$ for conventional InGaAs) provides 80% quantum efficiency. The use of a thin InGaAs absorber also implies low dark current, since a reduction in diffusion currents that limits conventional InGaAs photodiodes is expected [13].

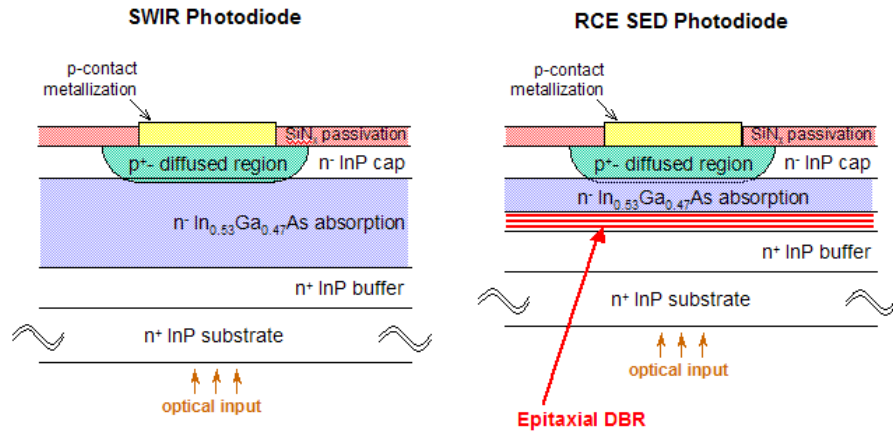


Figure 5: a) Cross-section of current state of art InGaAs photodiode pixel for SWIR imaging (left) and b) the proposed InGaAs RCE photodiode (sub-pixel) for SED (right).

Initial modeling results have been performed confirming the feasibility of the proposed technology. These results demonstrate a manufacturable design that has reasonable tolerance to fabrication process variations, ensuring high yield for high volume deployment. In the examples shown above, an FPA with 8 pixels tuned to different wavelengths, manufactured monolithically on a common substrate in a photodiode array were described. The number of wavelengths that can be incorporated into an array can be increased at the expense of escalating fabrication complexity. Each additional wavelength desired requires one additional photolithographic processing step.

2.4 SWIR explosives detection system configuration and capability

Based on the SWIR spectral characteristics of explosives described in section 2.1, a spectral analysis of a narrow spectral band from 1550nm-1800nm is sufficient for a high confidence level to detect EPs from a standoff distance. Based on the commercial InGaAs FPA fabrication technology, the monolithic InGaAs RCE photodiode array is hybridized to a commercial readout integrated circuit (ROIC) and is hermetically packaged. The FPA is then integrated with a custom built camera that stores digital corrections and detection algorithms for the SED imaging system. The ROIC can provide fast image acquisitions at minimum of 30 frames/sec. We anticipate that the explosive detection algorithms that will be incorporated in the custom camera electronics will perform comparison of relative pixel responses within a scene within the integration time, providing real time explosives detection capability. As an added benefit, the FPA does not require cooling systems since it is room temperature stabilized via an integrated TEC, hence consuming low power.

The SED system should operate in daylight conditions. In low-light level environments such as night or low illumination indoors, the system may use an eyesafe illuminator that is invisible to the human eye (wavelengths longer than 1550nm). This makes the system safe for users and individuals being interrogated, and also ensures covert operation, since it is invisible to the human eye and even conventional image intensified night vision goggles. Semiconductor lasers, LEDs or filtered lamps may be used as illumination sources

Table 1 below shows the potential capability of our proposed technology based on our initial calculations and simulation results. We have provided metrics for different configurations to highlight the trade-offs that are associated with employing the system.

Table 1. Potential capability of proposed technology based on initial calculations and simulation results.

POTENTIAL CAPABILITY	METRIC
Standoff range in meters	Lens A: A trace particle of 9 micro-grams can be detected at 0.5m A trace particle of 73 milligrams can be detected at 10m A trace particle of 0.58 grams can be detected at 20m Lens B: A trace particle of 0.78 micro-grams can be detected at 0.5m A trace particle of 6.2 milligrams can be detected at 10m A trace particle of 50 milligrams can be detected at 20m Lens C: A trace particle of 3.6 nano-grams can be detected at 0.5m A trace particle of 0.3 micro-grams can be detected at 10m A trace particle of 0.23 milligrams can be detected at 20m
Explosives detected	HMX, TNT, RDX, TATP, AN
Background materials compared against	Cotton, wood, cardboard, jeans, nylon (backpack), dark (no signal)
Sensitivity	Probability of detection (per integration time) = 89% Probability of false alarm (per integration time) = 12%
Selectivity (differentiation between explosives)	Probability of determining explosive type= 71%
Use in non-laboratory environments	Yes. May require simple calibration for use with different illumination or ambient light sources.
Projected sampling rate and spot size	Integration time is 32ms , imager running at 30Hz.
Eye safety aspects (wavelength, power)	Under sufficient ambient light, no illumination is required (passive). Under low light level conditions, an eye safe illumination source may be used at power levels indicated above.
Feasibility for nondestructive sampling	Yes, detection technique is non-destructive
Anticipated system dimensions and weight	Camera: 8.0 in x 5.0 in x 5.0 in and weight is < 4 lbs Lens A: 3.0 in x 2.0 (in diameter) and weight is < 0.5lbs Lens B: 8.6 in x 5.8 (in diameter) and weight is < 11.25 lbs Lens C: 12.6 in x 10 (in diameter) and weight is < 32.5 lbs Note: Above lenses were selected based on COTS Lenses. Significant reduction in size and weight is anticipated for a custom built lens (~50% reduction) for volume applications.
Power Consumption	< 3 Watts at room temperature

3. CALCULATION OF DETECTION PROBABILITY AND FALSE ALARM RATE:

Below we describe how we calculate detection probability and false alarm analysis using our invention. For each type of explosives we wish to detect, an algorithm calculates the similarity score (S_j) based on the detected super-pixel signals (δ_{ij}) and compares to the pre-programmed spectral characteristic (T_{ij}). The more “similar” the channel signals are to the preprogrammed values, the higher the similarity score value S_j .

$$S_j = A' - A \sum_{i=1}^{ic} \left| T_{ij} - \frac{\delta_{ij}}{\sum \delta_{ij}} \right| \quad (3)$$

- Such that:
- A' is an arbitrary constant.
 - A is a positive arbitrary constant
 - number of channels in a super-pixel: $i = [1, 2, 3, \dots 8]$
 - δ_i : signal at channel "i"
 - Number of EPs investigated for detection: $j = [1, 2, 3, \dots 5]$
 - S_j: similarity score (compared to a known EP characteristic)
 - T_{ij}: preprogrammed weight for channel i, EP type j. T_{ij} = {0,1}

Table 2 shows the calculated similarity scores for our 8-channel photodiode array example. Each detection algorithm (ex: S(HMX), S(TNT)) compares the similarity of an imaged material to the EP it was programmed for (HMX, TNT) using algorithm (3). Imaged background materials in this analysis materials are cotton, cardboard, wood, jeans, nylon or dark (no signal). The higher the similarity the detected signal is to the pre-programmed EP, the closer the number is to "1". If the similarity score is above a threshold, then the algorithm is considered to have found and material that matches an EP. The threshold must be chosen to give low incidences of false alarms while ensuring high EP detection probability. For example; in Table 2, when S(HMX) algorithm is used to analyze an image with jeans, the result is 0.57. If we select the threshold to be 0.9, the algorithm will not produce a false positive when imaging any of the background materials since they produce a value all less than the threshold. When imaging HMX, the result is "1", above the threshold, indicating a perfect match.

Table 2. Calculated similarity scores using described algorithm.

Detection Algorithm	Imaged material										
	Background Materials						Explosive Materials				
	Cotton	Cardb	Wood	Jeans	Nylon	Dark	HMX	TNT	RDX	TATP	AN
S(HMX)	0.72	0.65	0.70	0.57	0.84	0.73	1	0.83	0.85	0.90	0.06
S(TNT)	0.76	0.72	0.72	0.63	0.70	0.76	0.83	1	0.89	0.87	0.14
S(RDX)	0.72	0.65	0.68	0.56	0.71	0.73	0.85	0.89	1	0.89	0.05
S(TATP)	0.67	0.60	0.65	0.53	0.76	0.67	0.90	0.87	0.89	1	0.01
S(AN)	0.31	0.36	0.29	0.36	0.05	0.31	0.06	0.14	0.05	0.01	1

To simulate detection probability and false alarm rate analysis, a random intensity noise was added to the response of each channel of 20% (+/- 10%, uniformly distributed). This approximation is based on shot-noise limited imager characteristics, which represent a worst case. Our simulations were run for consecutive occurrences and we counted correct and false detections of EP compared to background materials such as cotton, wood, jeans, etc. When an EP is present, the system was able to correctly identify that EP was present on 49 occasions and was not able to identify the presence in 6 occurrences, yielding a detection probability of **89%**. When imaging a background material, the system was able to correctly identify that EP was **NOT** present on 57 occasions and produced false EP presence in 8 occurrences, yielding a false alarm probability of **12%**. In addition, the algorithm detected the presence of EP *AND* yielded its correct type of EP on 25 occurrences, while not detecting EP *OR* indicating the wrong type of EP 10 times. Therefore, probability of determining the explosive type = **71%**.

Note: The results shown above are initial attempts to assess system capability. By optimization of algorithm parameters and FPA design, better performance should be achieved. In addition, the probabilities of detection are for a single 32 msec integration time image acquisition. By evaluating multiple positives either spatially or temporally, the system can achieve a higher confidence in the detection of explosive traces.

4. CALCULATION OF STANDOFF DETECTION CAPABILITY:

Our goal in the following calculations is to predict the standoff EP detection capability of the FPA using commercially available SWIR lenses [15]. Significant reduction in size and weight is anticipated for a custom built lens (~50% reduction) by designing the optical system for this specific application.

A schematic of the optical system used in the application is shown below in Figure 6. We calculated the dimensions that are imaged onto a super-pixel at different standoff distances using existing lens properties. The following assumptions were made in this analysis:

- Use FPA design with 8 channels, 15µm pixel size pitch in a 3x3 configuration with 45µm X 45µm super-pixel size (one channel is not used in the 3x3). The imager format used is 1280x1024.
- The minimum size particle that the FPA can detect is limited by its projected image via the optical system being no smaller than a super-pixel of the FPA.
- Adequate illumination is present such that SNR is sufficient for the system
- Density of an EP is assumed 1.04 grams/cc, and the particle is spherical. The weight of the EP particle is calculated (in grams) to determine the detectable trace amount

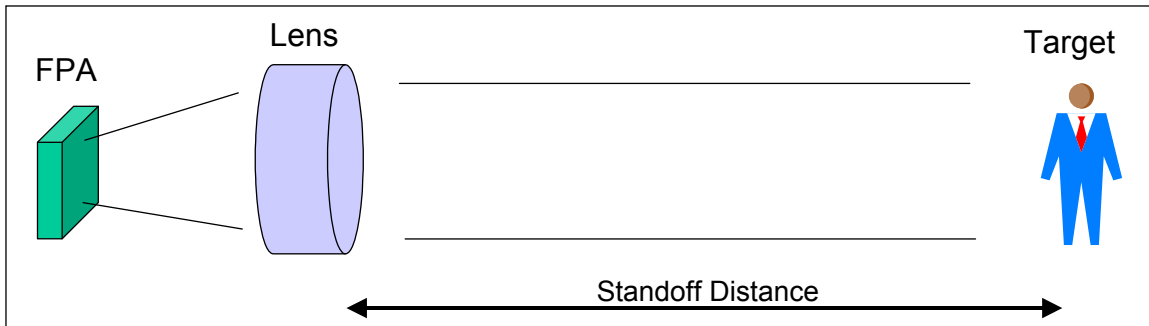


Figure 6. Schematic of the optical system used in the application of on standoff explosives detection.

Results of our calculations are shown in Table 3. The Field of view (FOV) in degrees for Lens A, Lens B, and Lens C are approximately 13, 6, and 2 respectively. Therefore, one must consider the FOV in designing the optical system for specific applications.

Table 3. Calculation of optical lens system on detectable particle size based at various stand-off distances.

	Optical Lens Properties				Detectable EM particles (in grams) at Standoff Distance (in m)					
	Focal Length (mm)	F #	Dimensions (length x diameter) mm	lens weight	1	5	10	15	20	50
Lens A	88	2	81 x 52 (3x2inches) 149 x 219	< 227 grams (0.5lbs)	7.3E-05	9.1E-03	7.3E-02	2.5E-01	5.8E-01	9.1E+00
Lens B	200	1.6	(8.6x5.8inches) 322 x 263	< 11.25 lbs	6.2E-06	7.8E-04	6.2E-03	2.1E-02	5.0E-02	7.8E-01
Lens C	1200	5	(12.6x10inches)	< 32.5 lbs	2.9E-08	3.6E-06	2.9E-05	9.7E-05	2.3E-04	3.6E-03

5. CONCLUSIONS

We have described our modeling and simulation results of a novel FPA designed to detect explosives at a large stand-off distance based on a SWIR hyperspectral imaging FPA. The proposed technology combines

conventional uncooled InGaAs based SWIR imaging with the wavelength selectivity of a monolithically integrated solid-state Fabry-Perot interferometer. The camera compares the spectral characteristics of explosives in the SWIR to detect and locate them within an imaged scene among various background materials. The technology will be compact, and consume low power such that it can be used as a handheld device and is ideal for unmanned vehicles. The technology does not use any scanning nor tuning apparatuses such as MEMS devices, and is therefore fast, compact, lightweight and not susceptible to vibration. We have presented a detailed design of the novel focal plane array and a calculated standoff distance, detection probabilities and false rates study under sufficient illumination conditions.

6. ACKNOWLEDGEMENTS

The authors would like to thank Ray Balcerak and Stuart Horn from Defense Advanced Research Projects Agency (DARPA) for fruitful discussions.

REFERENCES

- [1] National Research Council (NRC), "Existing and Potential Standoff Explosives Detection Techniques", National Academies Press, 2004.
- [2] Department of Homeland Security Science & Technology Counter-Improvised Explosives Detection (C-IED) Industry Outreach Workshop, Arlington, VA, December 10, 2008.
- [3] Klunder G., "Stand-off Detection of High Explosives with Near Infrared Spectroscopy", FACSS, September 2006.
- [4] M. Gaft, L. Nagli, "Standoff laser-based spectroscopy for explosives detection", Proc. SPIE, Vol. 6739, 673903 (2007)
- [5] V. Farley et. al., "Chemical Agent Detection With A Hyperspectral Imaging Infrared Sensor", Proc. SPIE Vol 6739-45 (2007).
- [6] Carver G.E., Entwistle M., Knurek C., Koch T., Lyons D., Owens M., Rangwala S., Salvemini D., "A New Dual Band Line Scan Camera for Rapid Inspection," The Vision Show East, Automated Imaging Association, Boston, MA, 2006
- [7] Wooten F., "Optical Properties of Solids", New York: Academic Press, pp. 47, 1972
- [8] Isbell, R.A., Brewster, M.Q., "Optical Properties of Energetic Materials: RDX, HMX, AP, NC/NG, and HTPB," Propellants, Explosives, Pyrotechnics, vol. 23, p. 218, 1998.
- [9] Hale G.M., Querry M.R., "Optical constants of water in the 200nm to 200 μ m wavelength region," Applied Optics, 12, p. 555, 1973.
- [10] Wolfe W.L., "Handbook of Military Infrared Technology," Naval Research Laboratory, p. 182, 1965.
- [11] M. S. Unlu et. al., "Resonant cavity enhanced photonic devices", Journal of Applied Physics, 78(2) 15 July 1995.
- [12] B. M. Onat and M. S. Unlu, "Polarization Sensing with Resonant Cavity Enhanced Photodetectors," IEEE Journal of Selected Topics in Quantum Electronics on Smart Pixels, Vol. 2(1), pp. 135-40, (1996).
- [13] B. M. Onat, et.al. "Ultra low dark current InGaAs technology for focal plane arrays for low light level visible-shortwave infrared imaging", *Proceedings of SPIE*, DSS Conference, Vol. 6542, pp. 6542OL-1, April. 2007
- [14] M. Enriquez, M. Blessinger, J. V. Groppe, T. M. Sudol, J. Battaglia, J. Passe, M. Stern, B. M. Onat, "Performance of high resolution Visible-InGaAs Imager for day/night vision", *Proceedings of SPIE*, DSS Conference, Vol. 6940, pp. 69400O-1, April. 2008
- [15] StingRay optics, www.stingrayoptics.com